Downsizing Porphyrin Covalent Organic Framework Particles Using Protected Precursors for Electrocatalytic CO_2 Reduction

Kenichi Endo[#], Asif Raza[#,†], Liang Yao[#,*], Samuel Van Gele[#,§], Andrés Rodríguez-Camargo[#,&], Hugo A. Vignolo-González[#,§,¶], Lars Grunenberg[#,§], Bettina V. Lotsch[#,§,¶,*]

[#] Nanochemistry Department, Max Planck Institute for Solid State Research, 70569 Stuttgart, Germany
[§] Department of Chemistry, Ludwig Maximilians University Munich, 81377 Munich, Germany
[&] Department of Chemistry, University of Stuttgart, 70569 Stuttgart, Germany
[¶] Cluster of Excellence e-conversion, 85748 Garching, Germany

SUBJECTS: Covalent organic frameworks, Morphology control, Electrochemical CO_2 reduction, Electrocatalysis, Porphyrin

ABSTRACT: Covalent organic frameworks (COFs) are promising electrocatalyst platforms owing to their designability, porosity, and stability. Recently, COFs with various chemical structures were developed as efficient electrochemical CO_2 reduction catalysts. However, controlling the morphology of COF catalysts remains a challenge, which can limit their electrocatalytic performance even if the chemical structure is optimally designed. Especially, while metalated porphyrinoids show great promise as catalytically active COF building blocks, their intermolecular stacking and coordination interactions make it difficult to conduct solution-based COF synthesis which can control the particle size dominated by the aggregation of crystallites. In this work, we report a new synthetic methodology for rationally downsized COF catalyst particles, where a tritylated amine is employed as a novel protected precursor for COF synthesis. Trityl protection provides high solubility to a representative cobalt porphyrin precursor, while its deprotection proceeds *in situ* under typical solvothermal COF synthesis conditions. This colloidal deprotection–polycondensation process yields smaller COF particles with less crystallite aggregation than a conventional synthesis, maintaining crystallinity and porosity. The downsized COF particles exhibit superior catalytic performance in electrochemical CO_2 reduction, with higher CO production rate and faradaic efficiency with similar stability compared to conventional COF particles. The improved performance of downsized COF particles is attributed to the higher contact area with a conductive agent. This study provides a strategy for the preparation of COF electrocatalysts with controlled morphology and enhanced performance and also reveals an important factor in the evaluation of COF electrocatalysts.

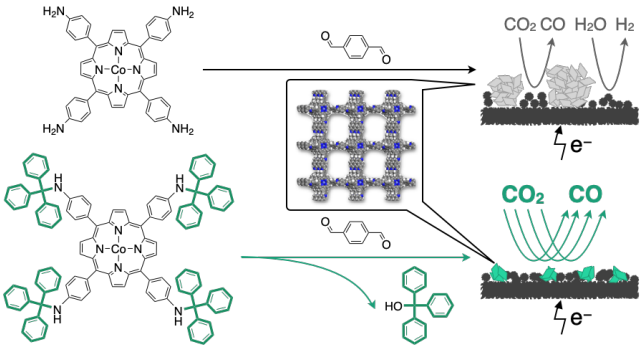

INTRODUCTION

Covalent organic frameworks (COFs), organic crystalline 2D or 3D polymers formed by reversible linkages,[1] are promising platforms for heterogeneous catalysis owing to their high chemical and topological designability, tunable porosity, and stability.[2] The exploration of COFs for electrocatalysis has recently gained interest because of the impetus for a transition to renewable energy sources.[3] COF electrocatalysts show promise in important reactions such as the hydrogen evolution, the oxygen evolution, the oxygen reduction, and the electrochemical CO_2 reduction reactions (HER, OER, ORR, and eCO_2RR, respectively). Among them, eCO_2RR has gained interest as a technology for closing the carbon cycle.[4-5] Since the first report of COF-catalyzed eCO_2RR by Chang, Yaghi, and co-workers in 2015,[6] a variety of COFs with different chemical structures have been developed affording remarkable eCO_2RR activity and selectivity for eCO_2RR over hydrogen evolution.[7] Among the reported COF eCO_2RR catalysts, metalated porphyrin- and phthalocyanine-based COFs have demonstrated the superiority of combining high activity and >90% selectivity even in aqueous electrolytes, where hydrogen evolution from water reduction can severely compete with eCO_2RR.[8] However, despite great success in the chemical structure design, morphology control at the COF micro- and macrostructure level remains largely unexplored. Most COF catalysts are obtained and used as large particles resulting from uncontrolled aggregation and intergrowth of small crystallites. Meanwhile, studies on other organic heterogeneous eCO_2RR catalysts have revealed that smaller particle sizes improve catalytic performance because charge transport to the active sites becomes more efficient.[9]

Therefore, downsizing COF particles is also expected to improve catalytic activity, and such studies on particle size effects are necessary to reveal the intrinsic catalytic properties of COFs.

Controlling the aggregation of COF crystallites represents one of the major challenges in the COF field, and several approaches have been developed over the past decade.[10] COF particles with sizes ranging from 10 nm to 1 μm based on boronate, imine, or ketoenamine linkages have been reported by using appropriate solvents,[11-14] low temperatures,[15-16] modulators,[17] surfactants,[18-19] or protecting groups.[19] However, it is worth mentioning that these strategies for suppressing aggregation usually have as a common prerequisite that all the COF precursors need to be dissolved to form a homogeneous solution. Meanwhile, metalated porphyrins and phthalocyanines, which are typically used for constructing eCO_2RR-active COFs, have a strong tendency toward intermolecular stacking and coordination. Although the weak intermolecular stacking of some COF precursors in solution can be utilized for morphology control,[14] the strong intermolecular interactions of porphyrins and phthalocyanines usually preclude their complete dissolution and thus hamper morphology control. Therefore, the morphology control of eCO_2RR-active COF particles remains challenging.

Herein, we introduce a novel synthetic approach for controlling the morphology of porphyrin COF catalysts that utilizes the trityl protection of amino groups (Figure 1). Trityl protection provides excellent solubility to a cobalt porphyrin precursor. Although trityl protection has never been employed in COF chemistry, we show that its deprotection proceeds *in situ* smoothly under typical COF synthesis conditions. This colloidal deprotection–polycondensation process offers downsized COF particles with less crystallite aggregation compared to the conventional unprotected precursor, without compromising the COF crystallinity and porosity. The downsized COF particles exhibit superior performance in eCO_2RR compared to conventional large COF particles.

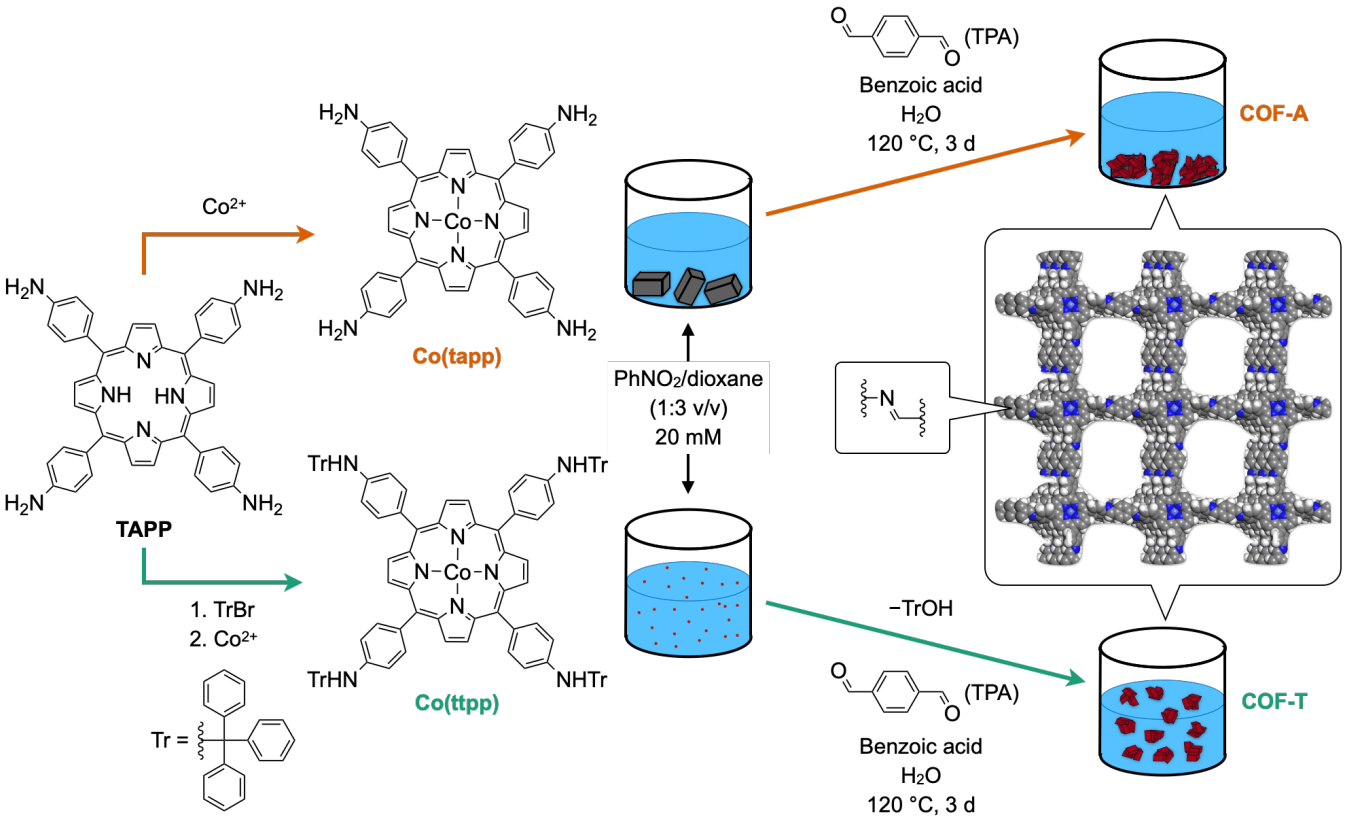

Figure 1. Synthetic schemes of downsized COF catalyst particles COF-T from a protected precursor Co(ttpp) in comparison with conventional COF particles COF-A from a conventional precursor Co(tapp), schematic representation of the dispersion states throughout the COF syntheses, and model crystal structure in a space-filling representation.

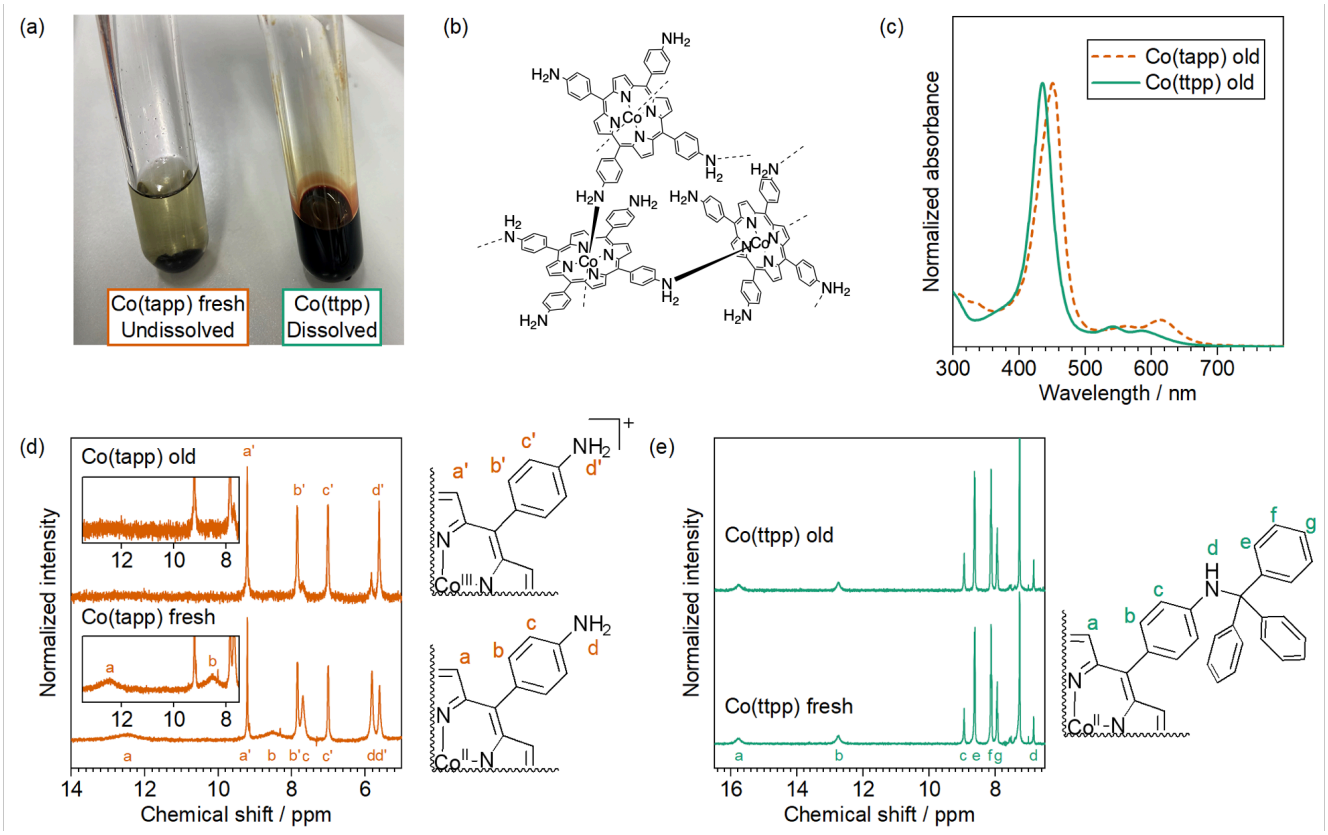

Figure 2. Characterization of Co(tapp) and Co(ttpp). (a) Photograph of a dissolution attempt (nitrobenzene/dioxane 1:3(v/v), nominally 20 mM, sonicated, room temperature). (b) Plausible chemical structure of undissolved Co(tapp). (c) UV–vis absorbance spectra of old samples left under air for 1 month (0.2 vol% pyridine/DMSO). (d) ^{1}H NMR spectra of fresh Co(tapp) and old Co(tapp) left under air for 1 month with assignments of signals (0.4 vol% piperidine/DMSO-d_6). The insets show magnification. (e) ^{1}H NMR spectra of fresh Co(ttpp) and old Co(ttpp) left under air for 1 month with assignments of signals ($CDCl_3$)

RESULTS AND DISCUSSION

Synthesis and characterization of a trityl-protected precursor Co(ttpp) and a conventional precursor Co(tapp). Co(tapp) (tapp = 5,10,15,20-tetrakis(4-aminophenyl)porphinato(2−)) is a precursor commonly used to synthesize COFs that catalyze electrochemical CO_2 reduction (Figure 1).[8] We noticed that Co(tapp) only partially dissolves under common COF synthesis conditions, which uses solvent mixtures such as *o*-dichlorobenzene/*n*-butanol 1:1(v/v)[6] or *o*-dichlorobenzene/benzyl alcohol 1:3(v/v)[20] at a nominal concentration around 10 mM and a temperature of 120 °C. The low solubility of Co(tapp) can be a general problem in the morphology control of its COF derivatives. Therefore, we aimed at improving the solubility of Co(tapp) using a protecting group.

We chose the trityl (Tr) group as a protecting group for Co(tapp). Bulky Tr groups are expected to effectively block the stacking of porphyrins, while they can be introduced and removed under mild conditions. Although tritylamines have never been employed in COF synthesis, they can be deprotected by acetic acid and water,[21-22] both of which are present in typical COF synthesis conditions. In addition, the deprotection is thermodynamically irreversible in the presence of 1 equiv. of water, yielding TrOH as a byproduct.[23] This behavior would promote burst nucleation after an initial deprotection stage, in contrast to the suppression of nucleation by competitive modulators typically used for obtaining larger crystallites.[24-25]

The four-fold Tr-protected Co(tapp), named Co(ttpp) (ttpp = 5,10,15,20-tetrakis(4-(tritylamino)phenyl)porphinato(2−)), is synthesized from free-base TAPP, which is the same precursor to Co(tapp) (Figure 1). Tritylation with TrBr and metalation with a Co^{2+} salt proceed successively in one pot, requiring no additional purification step. The product identity and purity are confirmed by ^{1}H nuclear magnetic resonance (NMR), electrospray ionization mass spectrometry (ESI-MS), infrared (IR) absorbance, ultraviolet–visible (UV–vis) absorbance, and inductively coupled plasma optical emission spectroscopy (ICP-OES) (Supporting Information page 7, Figures S3, S5, S6).

The solubility of Co(ttpp) was tested in various solvents. Co(ttpp) dissolves in a wide range of aprotic organic solvents (benzene, dichlorobenzene, nitrobenzene, dichloromethane, chloroform) at a concentration of more than 10 mM at room temperature. In nitrobenzene/dioxane 1:3(v/v), which is the optimal solvent for our COF synthesis (*vide infra*), Co(ttpp) is completely dissolved at a concentration of 20 mM while Co(tapp) is almost insoluble (Figure 2a). To investigate the origins of the improved solubility of Co(ttpp), we compare solubility in three cases. First, free-base TTPP dissolves in chloroform at a concentration of 10 mM while the solubility of TAPP is lower, which assures that the bulky Tr groups inhibit the

stacking of porphyrin rings and thus improve the solubility. Second, while TAPP dissolves in chloroform at a concentration of 0.5 mM, Co(tapp) is almost insoluble, indicating that the cobalt ion also plays a role in solubility. It is reported that cobalt porphyrins bearing amino or pyridyl groups form polymers via axial coordination at the cobalt centers,[26-27] suggesting similar coordination polymerization for Co(tapp) (Figure 2b). The bulky Tr groups in Co(ttpp) would inhibit such coordination and thus improve solubility. Third, Co(tapp) samples stored under air for a long time dissolve less than fresh samples, suggesting possible effects from the aerobic oxidation of Co(tapp).

To check the oxidation state of cobalt, we analyzed Co(tapp) and Co(ttpp) samples stored under air for 1 month or oxidized with I_2 by ^{1}H NMR and UV–vis absorbance spectroscopy. The ^{1}H NMR spectra of Co(tapp) samples show two sets of signals, which can be assigned to paramagnetic Co^{II} and diamagnetic Co^{III} species by comparison with the literature[28-29] (Figure 2d). An aged sample shows a higher amount of Co^{III} than a fresh sample, indicating gradual aerobic oxidation. In contrast, the ^{1}H NMR spectra of both fresh and old Co(ttpp) samples show only Co^{II} signals[28] (Figure 2e), and the absence of Co^{III} species is confirmed by comparison to a sample oxidized by I_2 (Figure S4). In the UV–vis absorbance spectra, old Co(tapp) shows a redshifted Soret band compared to that of Co(ttpp) (Figure 2c). The redshift can be attributed to the oxidation of Co^{II} to Co^{III},[30] which is supported by the spectrum of Co(ttpp) oxidized by I_2 (Figure S6). These results indicate that Co(tapp) is susceptible to aerobic oxidation while Co(ttpp) is stable. The oxidation of Co(tapp) would be promoted by the coordination of amino groups to cobalt, while the stability of Co(ttpp) is similar to a typical tetracoordinate cobalt porphyrin.[31] We could not obtain Co(tapp) in a pure Co^{II} state, even with an as-synthesized sample (Figure 2d), a commercial source of Co(tapp), or after treatment with $NaBH_4$.[32] Although the oxidation of Co(tapp) does not affect the resulting COF structure (*vide infra*), oxidation would strengthen the coordination of amino groups, lowering the solubility of Co(tapp).

To summarize, Tr-protected Co(ttpp) shows improved solubility by inhibiting porphyrin stacking, coordination polymerization, and aerobic oxidation observed in Co(tapp). The high solubility of Co(ttpp) is ideal for morphology-controlled COF syntheses. In this work, we focus on suppressing crystallite aggregation and decreasing the particle size which can be useful in three-dimensional electrodes for eCO_2RR.[4, 33-34]

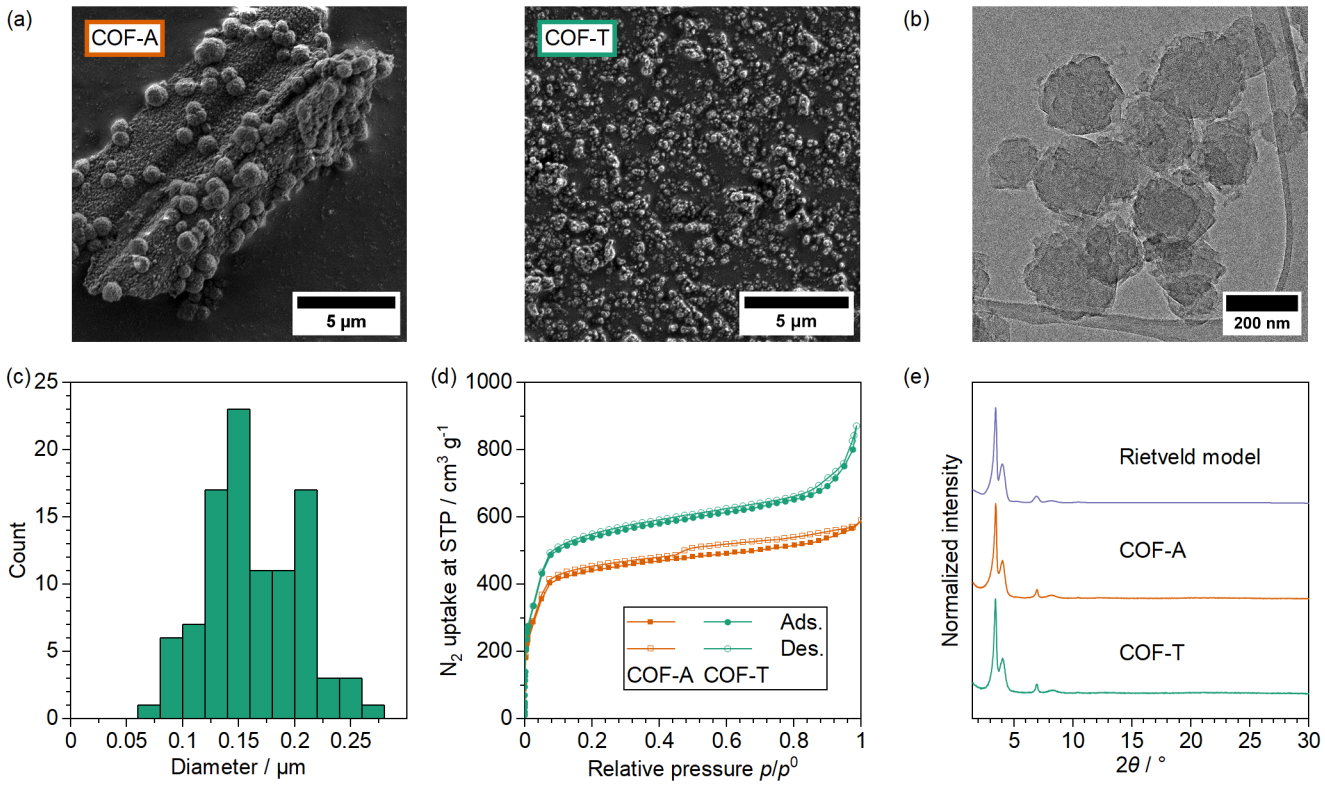

Figure 3. Comparison of structural characteristics of COF-A and COF-T. (a) SEM images. (b) TEM image of COF-T. (c) Particle size distribution of COF-T from TEM images (N = 100) (d) PXRD patterns (Cu Kα_1). (e) N_2 sorption isotherms (77 K).

Comparison of the COF formation from the unprotected vs. protected precursors. We chose COF-366-Co as a model porphyrin COF to synthesize because it is well-known as an eCO$_2$RR catalyst.[6, 35-36] COF-366-Co is a 2D square-lattice COF which forms from Co(tapp) and terephthalaldehyde (TPA) (Figure 1).

After optimization of the synthesis conditions, we found that COF-366-Co is formed as sub-µm particles when Co(ttpp) is solvothermally reacted with TPA in the presence of benzoic acid and water in nitrobenzene/dioxane 1:3(v/v). The solvent nitrobenzene/dioxane is advantageous to exploit the solubility of Co(ttpp), reaching more than 20 mM at room temperature, while two solvent systems typical in COF syntheses, mesitylene/dioxane 1:3 (v/v) and *o*-dichlorobenzene/*n*-butanol 1:1 (v/v), show less solubility. Acid and water promote reversible imine condensation as well as *in situ* deprotection of tritylamines. The product is hereafter called COF-T. For comparison, Co(tapp) was reacted with TPA under the same conditions, whose product is named COF-A.

The reactions of the two precursors give visual differences (Figure 1). Co(tapp) does not dissolve in the solvent even after sonication for 15 min and sediments at the bottom before heating, and the product COF-A is also found as a solid at the bottom. In contrast, Co(ttpp) completely dissolves in the solvent to form a homogeneous solution. After heating, the product COF-T solids are homogeneously suspended in the solvent, indicating that the reaction proceeds through colloidal states. The formation of a colloid is presumably due to the following two aspects: First, the homogenous initial state affords homogeneous nucleation. Second, rapid sedimentation of the growing COF can be inhibited by the high polarity of nitrobenzene solvent molecules, as seen in the colloidal COF synthesis in nitrile solvents.[11, 13-14, 37] These results mean that Tr protection changes the formation process of COF-366-Co from a solid-to-solid transformation to a solution-to-colloid process.

The product morphologies are analyzed by scanning electron microscopy (SEM), transmission electron microscopy (TEM), and powder X-ray diffraction (PXRD) in a powder state after filtration and rinsing with solvents and supercritical CO_2. In SEM images, COF-A shows rod-like particles with a size of around 10 µm, similar to that of Co(tapp) (Figure 3a, S8). While the surfaces of Co(tapp) particles before the reaction are smooth, the surfaces of COF-A particles are covered by many small crystallites and their spherical aggregates. This result indicates that COF-A grows on undissolved Co(tapp) particles by heterogeneous nucleation. On the other hand, SEM images of COF-T show only small spherical aggregates of crystallites, indicating that COF-T forms mainly from homogeneous nucleation from a solution (Figure 3a, S9). TEM images of COF-T show crystallite aggregates with diameters of 162 ± 41 nm (Figure 3b, S10), which is a two orders of magnitude smaller particle size than COF-A. Meanwhile, the crystallite (primary particle) sizes of COF-A and COF-T are similar, as indicated by the similar peak widths in PXRD patterns (Figure 3c). This result supports that the Tr groups in Co(ttpp) are irreversibly removed from the amino groups in the initial stage and do not interfere with crystal growth as modulators.[24-25]

The crystal structures of each sample are analyzed by PXRD and N_2 sorption. The PXRD patterns of COF-A and COF-T are

similar to each other and to a previous report of COF-366-Co,[6] indicating the formation of the same crystal structure (Figure 3c). Although the structure previously proposed was an eclipsed stacking model,[6] the presence of stacking slippage[38] is supported by further analysis with Rietveld refinement (Figure 1, Supporting Information pages 31–34). The PXRD patterns are also in a good agreement with the FFT of the TEM image of COF-T (Figure S10). The N_2 sorption isotherms of COF-A and COF-T show uptake curves in the microporous region similar to each other and to a previous report,[6] indicating similar micropore structures (Figure 3d). Accordingly, pore size distribution (PSD) analysis shows similar profiles with maxima at 2.1 nm for COF-A and COF-T (Figures S18, S19), which agrees with the model crystal structure (Figure S40). These results indicate that COF-A and COF-T have similar crystal structures despite the morphological differences, and Tr-protected amines work as a surrogate COF precursor without disturbing the crystal structure of the resultant COF.

The complete removal of Tr groups is further checked by solid-state ^{13}C NMR, digestion ^{1}H NMR, IR absorbance, and reaction yield. The solid-state ^{13}C NMR spectrum of COF-T is similar to that of COF-A, showing no signals from Tr groups (Figure S23). We also digested each COF into monomer solutions in DCl/D_2O/DMSO-d_6 solvent and analyzed them with ^{1}H NMR.[39] The ^{1}H NMR spectrum of digested COF-T shows only Co(tapp) and TPA signals similar to COF-A, without Tr species (Figures S20, S21). The solid-state ^{13}C NMR and IR absorbance spectra of COF-T are also similar to those of COF-A, showing no signals from Tr groups (Figures S22, S23). These results show that Tr groups are not incorporated into the COF, and the deprotection byproduct TrOH is removed by rinsing with solvents and supercritical CO_2. Meanwhile, the yield of COF-T is 87% from Co(ttpp) regarding the mass of cobalt determined by ICP-OES, with a small loss due to the particles trapped in the filter paper. The filtrate from the COF-T reaction mixture is pale orange in contrast to the dark red Co(ttpp) solution. These results indicate that the *in situ* deprotection of Co(ttpp) proceeds completely under these COF synthesis conditions.

The increased solubility of the precursor can also improve reaction progress. To investigate if this is the case, we analyze the digestion ^{1}H NMR, IR absorbance, and N_2 sorption data in detail. Integration of the TPA and Co(tapp) peaks in the digestion ^{1}H NMR spectra reveals their molar ratio, which should be 2 in pure COF-366-Co (Figures S20, S21). However, COF-A shows a TPA/Co(tapp) ratio of 1.66, while COF-T shows a TPA/Co(tapp) ratio of 1.99. This result indicates COF-A contains 17 mol% of unreacted Co(tapp). In the IR absorbance spectra, COF-A shows a weaker C=N stretch band than COF-T when normalized at the C=C stretch band, which supports the incomplete Co(tapp) conversion in COF-A (Figures S23). The N_2 sorption data show that COF-A adsorbs 15% less N_2 in micropores (Figure 3d, S13), has 18% less BET surface area (Figures S14–S18), and has 15% less micropore volume than COF-T. These values agree with the digestion ^{1}H NMR results, regarding unreacted Co(tapp) as a non-porous impurity and assuming COF micropores have similar accessibility reflecting similar crystallite sizes. To investigate the reason for incomplete conversion in COF-A, we tested two alternative sets of synthetic conditions. The use of excess TPA (3 equiv. to Co(tapp)) as in a previous report[6] results in an IR spectrum similar to COF-A (Figure S23), indicating similar incomplete conversion and ruling out the possibility that the consumption of TPA by side reactions is limiting the reaction progress. Increasing reaction time from 3 days to 9 days does not significantly change the product IR spectrum either (Figure S23). Therefore, we speculate that during the formation of COF-A, COF crystallites growing on the surfaces of undissolved Co(tapp) particles become passivation layers, leaving unreacted Co(tapp) cores. On the other hand, the high solubility of Co(ttpp) facilitates full conversion to a COF.

These results demonstrate that Co(ttpp) serves as a precursor to COF-366-Co via *in situ* deprotection, and the resulting COF-T preserves the crystal structure and crystallite size of COF-A from Co(tapp). Meanwhile, the higher solubility of Co(ttpp) than Co(tapp) enables the formation of smaller secondary particles. The smaller particle size of COF-T with a similar crystal structure and crystallite size to COF-A motivated us to study the effects of COF particle size on electrocatalytic performance.

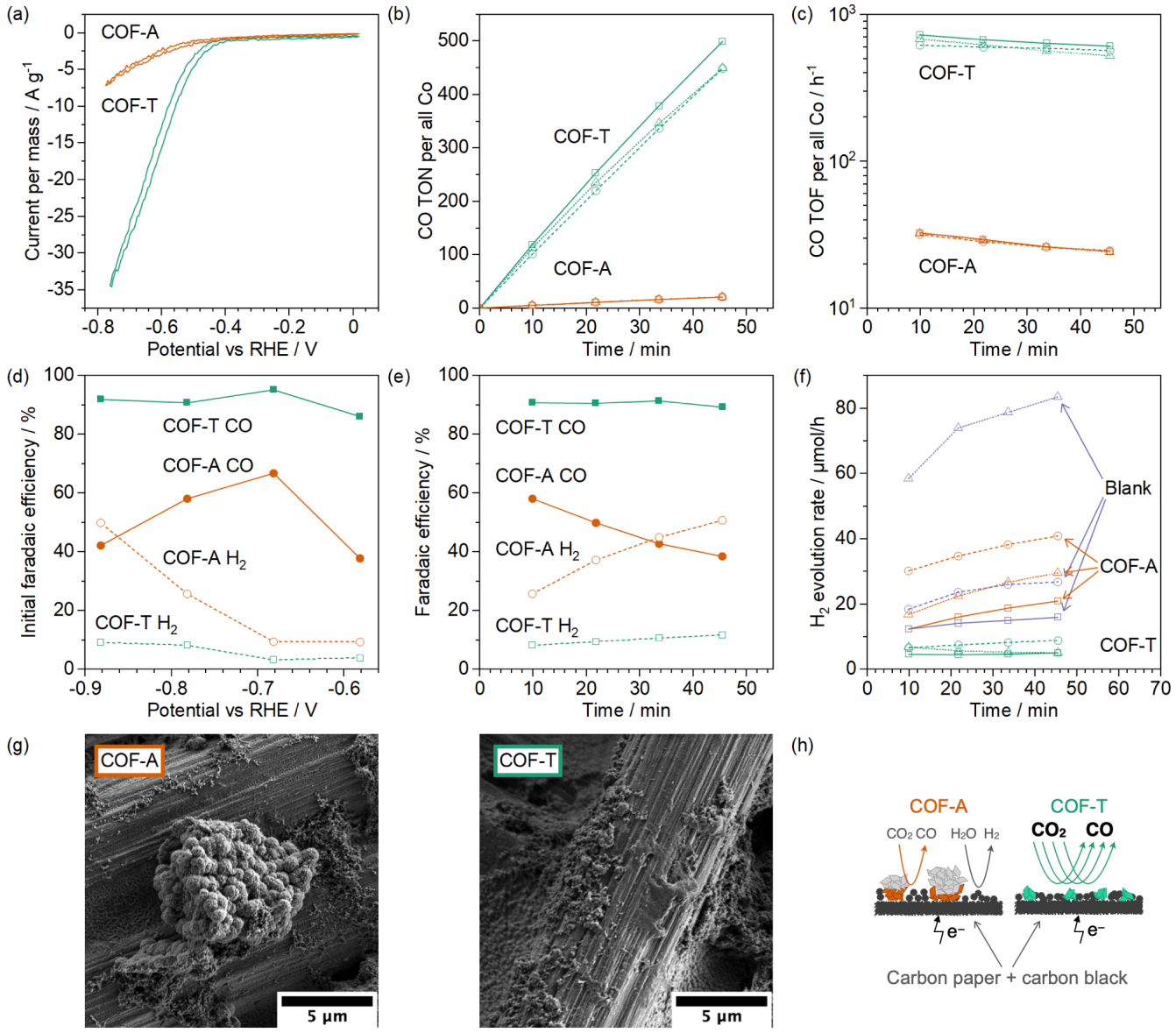

Figure 4. Electrochemical CO_2 reduction with COF-A and COF-T as catalysts (0.5 M $KHCO_3$ aq, CO_2 flow). (a) Cyclic voltammograms normalized by the mass of COF catalysts. (b) CO production turnover number (TON) per all cobalt atoms over time (−0.78 V vs RHE). Three measurements with different synthetic batches are shown for each material. (c) CO production turnover frequency (TOF) per all cobalt atoms over time (−0.78 V vs RHE, logarithmic scale). Three measurements with different synthetic batches are shown for each material. (d) Initial CO production faradaic efficiencies at different potentials (after headspace composition reaches a steady state in 10 min). (e) Faradaic efficiencies over time (−0.78 V vs RHE). (f) H_2 evolution rates over time in comparison with a blank electrode without COFs (−0.78 V vs RHE). Three measurements with different synthetic batches of COFs or different blank electrodes are shown for each material. (g) SEM images after electrolysis. (h) Schematic representation of the electrode structures and electrochemical reactions.

Electrochemical CO_2 reduction catalyzed by COFs from the unprotected and protected precursors. The catalytic properties of COF-A and COF-T for electrochemical CO_2 reduction are compared in 0.5 M aqueous $KHCO_3$ solution under CO_2 flow. The working electrodes were prepared with the same loading of a COF sample as a catalyst, carbon black as a conducting agent, and Nafion as a binder on pieces of carbon paper as current collectors. Cyclic voltammetry (CV) of the COF-A and COF-T electrodes shows catalytic currents at reductive potentials (Figure 4a). To quantify the catalysis products, potentiostatic electrolysis was conducted at certain potentials while the evolution of gaseous products was quantified by gas chromatography, and that of liquid products was checked by ^{1}H NMR. Both COFs give CO gas as the major product and H_2 gas as the only side product, while the formation of liquid products such as formate is negligible.

The catalytic activities of the COF-T and COF-A electrodes are compared in terms of CO production turnover frequency (TOF) per all cobalt. The COF-T electrode achieves a higher initial TOF than that of the COF-A electrode at a potential of −0.78 V vs the reversible hydrogen electrode (RHE) (Figure 4b,c). A similar enhancement in activity is observed over the

wide range of potentials from −0.88 V to −0.58 V vs RHE (Figure S24). Meanwhile, the catalytic stability of COF-T and COF-A electrodes are similar (Figure 4c, S25), and the higher activity of the COF-T electrode continues over 10 h (Figure S25). To check the possible interference by the unreacted Co(tapp) in COF-A, we also tested an electrode prepared from pristine Co(tapp). In our setup, pristine Co(tapp) shows higher activity than COF-A (Figure S26), indicating that the low activity of the COF-A electrode is not because of the unreacted Co(tapp) in COF-A. Therefore, it is demonstrated that particle downsizing can enhance the eCO_2RR activity of COFs significantly.

The faradaic efficiency (FE) of COF-T and COF-A electrodes are compared in Figure 4d and e. The COF-T electrode shows higher initial FE(CO) (86–95%) over a wide potential range from −0.58 V to −0.88 V vs RHE, while the COF-A electrode shows lower initial FE(CO) (38–67%). Moreover, the COF-T electrode exhibits better FE(CO) stability, maintaining a high FE(CO) of 89–91% for 45 min at −0.78 V vs RHE. In comparison, the FE(CO) of the COF-A electrode reduces from 58% to 38% under the same conditions, while $FE(H_2)$ increases from 26% to 51%. The lower selectivity of COF-A is not due to the unreacted Co(tapp), because the pristine Co(tapp) electrode shows higher FE(CO) (Figure S27). To investigate the origin of hydrogen evolution, we measured hydrogen evolution from a blank electrode without cobalt catalysts. Blank electrodes show H_2 evolution rates similar to COF-A and higher than COF-T electrodes, with a gradual increase in the H_2 evolution rate attributed to the electrowetting of the hydrophobic carbon materials (Figure 4f).[40] This result indicates that the small particles of COF-T suppress hydrogen evolution from electrode materials by efficient coverage, while the large particles of COF-A do not. Therefore, the higher FE(CO) of COF-T compared to COF-A is likely due to the suppression of hydrogen evolution from the electrode materials and the higher eCO_2RR activity from the COF-T particles.

We next carried out a series of characterizations to elucidate the origin of the superior electrocatalytic performance of COF-T. The electrode macrostructures are investigated by SEM as shown in Figure 4g, S29–S33. The COF-A electrode shows ~10 μm particles similar to the original COF-A particles sitting on the fibers of carbon paper both before and after electrolysis. In contrast, the COF-T electrode shows no large particles (> 1 μm) before and after electrolysis. Although the original particles of COF-T (~ 160 nm) are not clearly visible among carbon black particles (~ 50 nm), the PXRD and IR absorbance measurements of the COF-T/carbon black/Nafion catalyst ink show that the crystal and chemical structure of COF-T is maintained in the mixture (Figures S33, S34). Hence, it can be assumed that COF-T is well dispersed as small particles among carbon black on the electrode. A control experiment without carbon black shows a diminished CO evolution (Figure S28). These results indicate that efficient eCO_2RR occurs at the interface between COF particles and carbon black particles, as the conductivity of COFs is insufficient. Similar behavior is reported for other organic heterogeneous catalysts for eCO_2RR.[9, 41] In our system, the smaller particle size of COF-T compared to COF-A provides a larger interfacial area with carbon black (Figure 4h). In addition, the large particles of COF-A can disrupt or protrude from the carbon black layer, further diminishing the interface. Therefore, downsized COF-T particles show higher electrocatalytic activity.

CONCLUSIONS

In this work, we demonstrated a rational protocol for suppressing the crystallite aggregation of COF eCO_2RR catalysts, which enables the downsizing of COF-366-Co particles to hundreds of nanometers. The conventional synthesis of COF-366-Co is based on poorly soluble Co(tapp) and results in large crystallite aggregates with a size of around 10 μm because of heterogeneous nucleation, along with the incomplete conversion of Co(tapp) into the COF. By introducing trityl protection groups, the solubility of the porphyrin COF precursor, i.e. Co(ttpp), is significantly improved owing to the suppression of intermolecular stacking and amine-cobalt coordination interactions. The use of Co(ttpp) as a precursor affords homogeneous nucleation and downsizes COF-366-Co particles to 162 ± 41 nm, suppressing crystallite aggregation. It is worth mentioning that trityl groups can be introduced easily to amino groups and can be deprotected *in situ* under standard COF synthesis conditions, thus rendering the method introduced here generic and universal for many types of COFs. While the downsized COF particles obtained by this method are useful for electrode fabrication, they likewise apply to other scenarios in which colloidal processing and film formation is desired.[11, 14, 42] Highly soluble precursors are useful as well for other COF morphologies, such as the in-situ growth of oriented thin films.[19]

This work showcases the effects of crystallite aggregation and resultant particle size in COF electrocatalysts. The downsizing of COF-366-Co particles enhances eCO_2RR activity owing to the higher contact area with a conductive agent, achieving a higher CO production TOF compared to the larger particles obtained via the conventional approach. Therefore, particle downsizing has the potential to systematically and significantly improve the electrocatalytic performance of COFs. Finally, this insight implies that the effects of particle size should be always considered when different COF electrocatalysts are compared to reveal intrinsic structure–performance relationships.

ASSOCIATED CONTENT

Supporting Information

The Supporting Information is available free of charge on the ACS Publications website.

Methods, Supplementary Figures and Tables, Structure modeling and Rietveld refinement, and Supplementary references (PDF)

Structural model of COF-T (CIF)

N_2 adsorption data of COF-A and COF-T in the AIF format (ZIP)

AUTHOR INFORMATION

Corresponding Authors

Liang Yao – Email: l.yao@fkf.mpg.de
Bettina V. Lotsch – Email: b.lotsch@fkf.mpg.de

Present Addresses

[†]Bernal Institute, University of Limerick, V94 T9PX Limerick, Ireland

Notes

The authors declare no competing financial interest.

ACKNOWLEDGMENT

The authors thank Viola Duppel (MPI-FKF) for TEM imaging, Igor Moudrakovski (MPI-FKF) for solid-state NMR measurements, and Alexander M. Pütz (MPI-FKF) for BET analysis. K.E. acknowledges postdoctoral scholarships from the Max Planck Society and the Alexander von Humboldt Foundation. The authors acknowledge financial support from Deutsche Forschungsgemeinschaft (DFG, German Research Foundation, Project-ID 358283783, SFB 1333), Max-Planck-Gesellschaft, Center for NanoScience (Ludwig-Maximilians-Universität München), Exzellenzclusters e-conversion (EXC 2089/1–390776260), and Solar Technologies go Hybrid (SolTech, Bavarian Research Network).

REFERENCES

1. Diercks, C. S.; Yaghi, O. M., The atom, the molecule, and the covalent organic framework. *Science* **2017,** *355* (6328), eaal1585.
2. Yusran, Y.; Li, H.; Guan, X.; Fang, Q.; Qiu, S., Covalent Organic Frameworks for Catalysis. *EnergyChem* **2020,** *2* (3), 100035.
3. Zhao, X.; Pachfule, P.; Thomas, A., Covalent organic frameworks (COFs) for electrochemical applications. *Chem. Soc. Rev.* **2021,** *50*, 6871-6913.
4. Wang, G.; Chen, J.; Ding, Y.; Cai, P.; Yi, L.; Li, Y.; Tu, C.; Hou, Y.; Wen, Z.; Dai, L., Electrocatalysis for CO2 conversion: from fundamentals to value-added products. *Chem. Soc. Rev.* **2021,** *50*, 4993-5061.
5. Overa, S.; Ko, B. H.; Zhao, Y.; Jiao, F., Electrochemical Approaches for CO(2) Conversion to Chemicals: A Journey toward Practical Applications. *Acc. Chem. Res.* **2022,** *55*, 638-648.
6. Lin, S.; Diercks, C. S.; Zhang, Y. B.; Kornienko, N.; Nichols, E. M.; Zhao, Y.; Paris, A. R.; Kim, D.; Yang, P.; Yaghi, O. M.; Chang, C. J., Covalent organic frameworks comprising cobalt porphyrins for catalytic CO(2) reduction in water. *Science* **2015,** *349*, 1208-13.
7. Fan, Y.; Chen, M.; Xu, N.; Wang, K.; Gao, Q.; Liang, J.; Liu, Y., Recent progress on covalent organic framework materials as CO(2) reduction electrocatalysts. *Front. Chem.* **2022,** *10*, 942492.
8. Huang, S.; Chen, K.; Li, T.-T., Porphyrin and phthalocyanine based covalent organic frameworks for electrocatalysis. *Coord. Chem. Rev.* **2022,** *464*, 214563.
9. Ren, S.; Lees, E. W.; Hunt, C.; Jewlal, A.; Kim, Y.; Zhang, Z.; Mowbray, B. A. W.; Fink, A. G.; Melo, L.; Grant, E. R.; Berlinguette, C. P., Catalyst Aggregation Matters for Immobilized Molecular CO(2)RR Electrocatalysts. *J. Am. Chem. Soc.* **2023,** *145* (8), 4414-4420.
10. Zhang, Z.; Zhang, L.; Wang, X.; Wang, T.; Cheng, C.; Liu, X., Micro/Nano‐Scaled Covalent Organic Frameworks: Polymerization, Crystallization and Self‐Assembly. *ChemNanoMat* **2021,** *8*, e202100345.
11. Smith, B. J.; Parent, L. R.; Overholts, A. C.; Beaucage, P. A.; Bisbey, R. P.; Chavez, A. D.; Hwang, N.; Park, C.; Evans, A. M.; Gianneschi, N. C.; Dichtel, W. R., Colloidal Covalent Organic Frameworks. *ACS Cent. Sci.* **2017,** *3* (1), 58-65.
12. Li, R. L.; Flanders, N. C.; Evans, A. M.; Ji, W.; Castano, I.; Chen, L. X.; Gianneschi, N. C.; Dichtel, W. R., Controlled growth of imine-linked two-dimensional covalent organic framework nanoparticles. *Chem. Sci.* **2019,** *10* (13), 3796-3801.
13. Evans, A. M.; Castano, I.; Brumberg, A.; Parent, L. R.; Corcos, A. R.; Li, R. L.; Flanders, N. C.; Gosztola, D. J.; Gianneschi, N. C.; Schaller, R. D.; Dichtel, W. R., Emissive Single-Crystalline Boroxine-Linked Colloidal Covalent Organic Frameworks. *J. Am. Chem. Soc.* **2019,** *141* (50), 19728-19735.
14. Yao, L.; Rodriguez-Camargo, A.; Xia, M.; Mucke, D.; Guntermann, R.; Liu, Y.; Grunenberg, L.; Jimenez-Solano, A.; Emmerling, S. T.; Duppel, V.; Sivula, K.; Bein, T.; Qi, H.; Kaiser, U.; Gratzel, M.; Lotsch, B. V., Covalent Organic Framework Nanoplates Enable Solution-Processed Crystalline Nanofilms for Photoelectrochemical Hydrogen Evolution. *J. Am. Chem. Soc.* **2022,** *144* (23), 10291-10300.
15. Yang, C. X.; Liu, C.; Cao, Y. M.; Yan, X. P., Facile room-temperature solution-phase synthesis of a spherical covalent organic framework for high-resolution chromatographic separation. *Chem. Commun.* **2015,** *51* (61), 12254-7.
16. Rodríguez-San-Miguel, D.; Corral-Pérez, J. J.; Gil-González, E.; Cuellas, D.; Arauzo, J.; Monsalvo, V. M.; Carcelén, V.; Zamora, F., Sub-micron spheres of an imine-based covalent organic framework: supramolecular functionalization and water-dispersibility. *CrystEngComm* **2017,** *19* (33), 4872-4876.
17. Gao, K. X.; Zhou, Z.; Yao, L.; Wang, S.; Zhang, Y.; Zou, Q.; Ma, L. X.; Wang, H. X., Aspartic Acid-Assisted Size-Controllable Synthesis of Nanoscale Spherical Covalent Organic Frameworks with Chiral Interfaces for Inhibiting Amyloid-beta Fibrillation. *ACS Appl. Bio. Mater.* **2022,** *5*, 1210-1221.
18. Franco, C.; Rodriguez-San-Miguel, D.; Sorrenti, A.; Sevim, S.; Pons, R.; Platero-Prats, A. E.; Pavlovic, M.; Szilagyi, I.; Ruiz Gonzalez, M. L.; Gonzalez-Calbet, J. M.; Bochicchio, D.; Pesce, L.; Pavan, G. M.; Imaz, I.; Cano-Sarabia, M.; Maspoch, D.; Pane, S.; de Mello, A. J.; Zamora, F.; Puigmarti-Luis, J., Biomimetic Synthesis of Sub-20 nm Covalent Organic Frameworks in Water. *J. Am. Chem. Soc.* **2020,** *142* (7), 3540-3547.
19. Zhao, Y.; Guo, L.; Gandara, F.; Ma, Y.; Liu, Z.; Zhu, C.; Lyu, H.; Trickett, C. A.; Kapustin, E. A.; Terasaki, O.; Yaghi, O. M., A Synthetic Route for Crystals of Woven Structures, Uniform Nanocrystals, and Thin Films of Imine Covalent Organic Frameworks. *J. Am. Chem. Soc.* **2017,** *139* (37), 13166-13172.
20. Wu, Q.; Xie, R.-K.; Mao, M.-J.; Chai, G.-L.; Yi, J.-D.; Zhao, S.-S.; Huang, Y.-B.; Cao, R., Integration of Strong Electron Transporter Tetrathiafulvalene into Metalloporphyrin-Based Covalent Organic Framework for Highly Efficient Electroreduction of CO2. *ACS Energy Lett.* **2020,** *5* (3), 1005-1012.
21. Dolence, E. K.; Morita, H.; Watt, D. S.; Fitz, T., Utilization of a nitrenium ion cyclization in a synthesis of a photoactive prostaglandin, 17-(4-azido-2-hydroxyphenyl)-18,19,20-trinorprostaglandin F2/ga. *Tetrahedron Lett.* **1987,** *28*, 43-46.
22. Kawada, K.; Dolence, E. K.; Morita, H.; Kometani, T.; Watt, D. S.; Balapure, A.; Fitz, T. A.; Orlicky, D. J.; Gerschenson, L. E., Prostaglandin photoaffinity probes: synthesis and biological activity of azide-substituted 16-phenoxy- and 17-phenyl-PGF2 alpha prostaglandins. *J. Med. Chem.* **1989,** *32*, 256-64.
23. Lu, R. J.; Liu, D.; Giese, R. W., Detritylation with ytterbium triflate. *Tetrahedron Lett.* **2000,** *41*, 2817-2819.
24. Ma, T.; Kapustin, E. A.; Yin, S. X.; Liang, L.; Zhou, Z.; Niu, J.; Li, L. H.; Wang, Y.; Su, J.; Li, J.; Wang, X.; Wang, W. D.; Wang, W.; Sun, J.; Yaghi, O. M., Single-crystal x-ray diffraction structures of covalent organic frameworks. *Science* **2018,** *361*, 48-52.
25. Calik, M.; Sick, T.; Dogru, M.; Doblinger, M.; Datz, S.; Budde, H.; Hartschuh, A.; Auras, F.; Bein, T., From Highly Crystalline to Outer Surface-Functionalized Covalent Organic Frameworks--A Modulation Approach. *J. Am. Chem. Soc.* **2016,** *138* (4), 1234-9.
26. Lin, K. J., SMTP-1: The First Functionalized Metalloporphyrin Molecular Sieves with Large Channels. *Angew. Chem. Int. Ed.* **1999,** *38* (18), 2730-2732.
27. Xiao, G.-B.; Yu, Z.-F.; Cao, J.; Tang, Y., Encapsulation and Regeneration of Perovskite Film by in Situ Forming Cobalt Porphyrin Polymer for Efficient Photovoltaics. *CCS Chemistry* **2020,** *2* (5), 488-494.
28. Medforth, C. J.; Hobbs, J. D.; Rodriguez, M. R.; Abraham, R. J.; Smith, K. M.; Shelnutt, J. A., Solution Conformations of Dodecasubstituted Cobalt(II) Porphyrins. *Inorg. Chem.* **2002,** *34*, 1333-1341.
29. Lin, M.; Marzilli, L. G., Solution Chemistry of Cobalt(III) Porphyrins in Water and Nonaqueous Solvents. Axial Ligation by Solvent and Counterion. *Inorg. Chem.* **2002,** *33*, 5309-5315.
30. D'Souza, F.; Villard, A.; Van Caemelbecke, E.; Franzen, M.; Boschi, T.; Tagliatesta, P.; Kadish, K. M., Electrochemical and spectroelectrochemical behavior of cobalt(III), cobalt(II), and cobalt(I) complexes of meso-tetraphenylporphyrinate bearing bromides on the .beta.-pyrrole positions. *Inorg. Chem.* **2002,** *32*, 4042-4048.
31. Shirazi, A.; Goff, H. M., Carbon-13 and proton NMR spectroscopy of four- and five-coordinate cobalt(II) porphyrins: analysis of NMR isotropic shifts. *Inorg. Chem.* **1982,** *21*, 3420-3425.
32. Gong, Y. N.; Zhong, W.; Li, Y.; Qiu, Y.; Zheng, L.; Jiang, J.; Jiang, H. L., Regulating Photocatalysis by Spin-State Manipulation of Cobalt in Covalent Organic Frameworks. *J. Am. Chem. Soc.* **2020,** *142* (39), 16723-16731.
33. Pan, F.; Yang, Y., Designing CO2 reduction electrode materials by morphology and interface engineering. *Energy Environ. Sci.* **2020,** *13* (8), 2275-2309.

34. Lees, E. W.; Mowbray, B. A. W.; Parlane, F. G. L.; Berlinguette, C. P., Gas diffusion electrodes and membranes for CO2 reduction electrolysers. *Nat. Rev. Mater.* **2021,** *7* (1), 55-64.
35. Diercks, C. S.; Lin, S.; Kornienko, N.; Kapustin, E. A.; Nichols, E. M.; Zhu, C.; Zhao, Y.; Chang, C. J.; Yaghi, O. M., Reticular Electronic Tuning of Porphyrin Active Sites in Covalent Organic Frameworks for Electrocatalytic Carbon Dioxide Reduction. *J. Am. Chem. Soc.* **2018,** *140* (3), 1116-1122.
36. Lu, Y.; Zhang, J.; Wei, W.; Ma, D. D.; Wu, X. T.; Zhu, Q. L., Efficient Carbon Dioxide Electroreduction over Ultrathin Covalent Organic Framework Nanolayers with Isolated Cobalt Porphyrin Units. *ACS Appl. Mater. Interfaces* **2020,** *12* (34), 37986-37992.
37. Natraj, A.; Ji, W.; Xin, J.; Castano, I.; Burke, D. W.; Evans, A. M.; Strauss, M. J.; Ateia, M.; Hamachi, L. S.; Gianneschi, N. C.; ZA, A. L.; Sun, J.; Yusuf, K.; Dichtel, W. R., Single-Crystalline Imine-Linked Two-Dimensional Covalent Organic Frameworks Separate Benzene and Cyclohexane Efficiently. *J. Am. Chem. Soc.* **2022,** *144* (43), 19813-19824.
38. Keller, N.; Calik, M.; Sharapa, D.; Soni, H. R.; Zehetmaier, P. M.; Rager, S.; Auras, F.; Jakowetz, A. C.; Gorling, A.; Clark, T.; Bein, T., Enforcing Extended Porphyrin J-Aggregate Stacking in Covalent Organic Frameworks. *J. Am. Chem. Soc.* **2018,** *140* (48), 16544-16552.
39. Zhao, S.; Dong, B.; Ge, R.; Wang, C.; Song, X.; Ma, W.; Wang, Y.; Hao, C.; Guo, X.; Gao, Y., Channel-wall functionalization in covalent organic frameworks for the enhancement of CO2 uptake and CO2/N2 selectivity. *RSC Advances* **2016,** *6* (45), 38774-38781.
40. Yang, K.; Kas, R.; Smith, W. A.; Burdyny, T., Role of the Carbon-Based Gas Diffusion Layer on Flooding in a Gas Diffusion Electrode Cell for Electrochemical CO2 Reduction. *ACS Energy Lett.* **2020,** *6* (1), 33-40.
41. Wu, Y.; Liang, Y.; Wang, H., Heterogeneous Molecular Catalysts of Metal Phthalocyanines for Electrochemical CO(2) Reduction Reactions. *Acc. Chem. Res.* **2021,** *54*, 3149–3159.
42. Evans, A. M.; Giri, A.; Sangwan, V. K.; Xun, S.; Bartnof, M.; Torres-Castanedo, C. G.; Balch, H. B.; Rahn, M. S.; Bradshaw, N. P.; Vitaku, E.; Burke, D. W.; Li, H.; Bedzyk, M. J.; Wang, F.; Bredas, J. L.; Malen, J. A.; McGaughey, A. J. H.; Hersam, M. C.; Dichtel, W. R.; Hopkins, P. E., Thermally conductive ultra-low-k dielectric layers based on two-dimensional covalent organic frameworks. *Nat. Mater.* **2021,** *20* (8), 1142-1148.